Construction and Building Materials 448 (2024) 138097

Contents lists available at ScienceDirect

Construction and Building Materials

journal homepage: www.elsevier.com/locate/conbuildmat

A versatile model with a design framework for axially-loaded FRP-confined concrete with/without a stress reduction-recovery behavior

Javad Shayanfar *, Joaquim A.O. Barros, João P.C. Pereira

Department of Civil Engineering, University of Minho, Azurém, Guimarães 4800-058, Portugal

ARTICLE INFO

Keywords:
Unified model
Design-oriented model
FRP-confined concrete
Strain softening behavior

ABSTRACT

Given the magnitude of investigations conducted on axially-loaded FRP-confined concrete columns in the past two decades, the focus of these studies was mainly given on FRP-confined concrete with a full strain hardening behavior, categorized as Type A. Nonetheless, for a reliable design of FRP confinement arrangements imposed to concrete, it is essential to properly comprehend and accurately simulate the mechanical behavior of FRP-confined concrete considering the possibility of a stress reduction-recovery response (Type B). Accordingly, this study proposes a new unified design-oriented model to predict the stress-strain behavior of axially-loaded FRP-confined normal/high-strength concrete cylinders with either Type A or Type B. The model consists of a two-segment stress-strain function for Type A whereas it, with a smooth transition, is transformed into a three-segment stress-strain function for Type B. A new parabolic stress-strain relation was developed for the first portion of axial behavior prior to the transition zone. Based on a new analytical methodology, new formulations with a design framework were proposed to predict the slope of softening/hardening linear functions, calibrated based on a large test database of Type A and Type B specimens. Furthermore, based on a reliable numerical database, simplified formulations are proposed to calculate the stress and strain at the transition zone of the stress-strain relations. The comparative assessment of the developed design-oriented model with existing confinement models reveals the developed one has not only superior predictive performance but also a simpler calculation process, which makes it suitable for design purposes by balancing the reliability and the implementation simplicity of the model.

1. Introduction

Considering the wide usage of fiber-reinforced-polymer (FRP) composites in the civil engineering and construction industry, their application as a confining material to reinforced concrete (RC) columns can potentially pose significant enhancements in terms of serviceability and collapse limit states [1]. Research studies regarding the axial and dilation behavior of FRP-confined concrete/RC columns have been under continuous conduction, particularly when a high-strength concrete (HSC) or ultra-high-strength concrete (UHSC) with FRP confinement is to be considered. Experimental studies ([1–10]) have evidenced that under axial compressive loading, FRP-confined concrete might exhibit a stress reduction-recovery behavior (post-peak strain softening-hardening behavior), as demonstrated in Fig. 1. Given the magnitude of investigations conducted on axially-loaded FRP-confined concrete columns in the past two decades, the focus of most of these studies was given on FRP-confined concrete with a full strain hardening behavior. Nonetheless, for a reliable design of FRP confinement arrangements imposed to concrete, it is essential to properly comprehend and accurately simulate the mechanical behavior of FRP-confined concrete considering the possibility of a stress reduction-recovery response.

Based on a review of existing experimental studies ([11–18]), factors influencing primarily the development of this phenomenon in the case of FRP-confined concrete of circular cross-section can be classified into three groups: i) the lateral confinement stiffness (K_L) imposed by FRP to the concrete elements; ii) the axial compressive strength of unconfined concrete (f_{c0}); and iii) the column size ($\beta_b = b/150$ where b is the diameter of a circular cross-section concrete column). Regarding the first group, a significant number of existing experimental studies investigated the effect of K_L on the mechanical properties of axially-loaded FRP-confined concrete columns. It was demonstrated by Eid *et al.* [19] that through providing a high level of K_L, concrete lateral

* Corresponding author.
E-mail addresses: arch3d.ir@gmail.com, id8287@alunos.uminho.pt (J. Shayanfar), barros@civil.uminho.pt (J.A.O. Barros), pg50484@alunos.uminho.pt (J.P.C. Pereira).

https://doi.org/10.1016/j.conbuildmat.2024.138097
Received 18 July 2024; Received in revised form 24 August 2024; Accepted 26 August 2024
Available online 6 September 2024
0950-0618/© 2024 Elsevier Ltd. All rights are reserved, including those for text and data mining, AI training, and similar technologies.

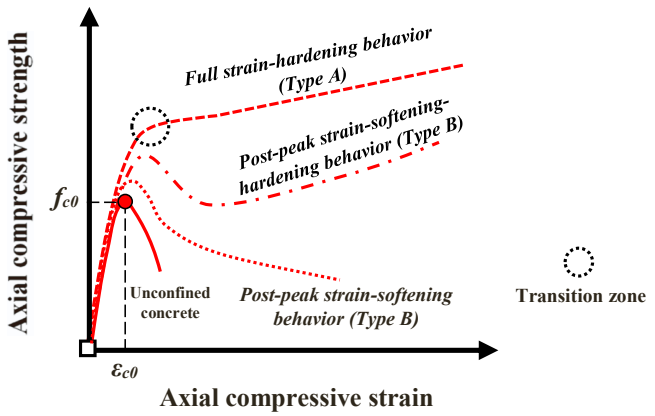


Fig. 1. Typical stress-strain behavior of axially-loaded FRP-confined concrete columns.

expansibility is strongly limited, which results in a full strain hardening response along with a substantial enhancement in axial stiffness, compressive strength, axial deformability, and energy dissipation. Nevertheless, by decreasing K_L the hardening character of FRP-confined concrete is altered to a strain-softening behavior beyond the transition zone (stress reduction response), followed by a hardening behavior (stress recovery response), Fig. 1. Furthermore, K_L is a main factor in the governing concrete cracking patterns, where a diffuse micro-cracking to a localized macro-cracking pattern can be obtained from a high to low level of K_L, as confirmed by [20–24]. Regarding the second group, the influence of f_{c0} on the mechanical properties of axially-loaded FRP-confined concrete columns was demonstrated by experimental studies conducted by Ozbakkaloglu and Akin [12], Vincent and Ozbakkaloglu [25], Demir *et al.* [26], Zeng *et al.* [17], and Liao *et al.* [27]. It was evidenced that the efficiency of an FRP confining system in terms of axial strength and strain ductility decreases by increasing f_{c0}, owing to confinement lagging, caused by the reduction of concrete lateral deformability with f_{c0}. Furthermore, Ozbakkaloglu and Akin [12] experimentally revealed that by increasing f_{c0}, a higher level of K_L is required to be imposed on the concrete to present a full strain hardening behavior during the entire axial loading process. Based on De Oliveira *et al.* [3], for cases having a strain-softening behavior (or a strain softening-hardening one) beyond the transition zone, the magnitude of the stress reduction is more pronounced for HSC/UHSC, with an abrupt gradient with axial strain, than normal-strength concrete (NSC). Regarding the third group, based on experimental investigations executed by Elsanadedy *et al.* [13], Zhou et al. [28], Wang *et al.* [15], Pessiki *et al.* [29], and Fan *et al.* [30], it was evidenced that there is no evident size effect for FRP-confined concrete columns with a full strain hardening behavior. However, a considerable size effect was observed for cases whose axial response has a strain-softening phase, leading to a deformation localization behavior. Besides β_b, the dominance degree of this effect is dependent on $K_L$and f_{c0} (Jamatia and Deb [31]).

To determine the stress-strain relationship of FRP-confined concrete, many analysis- and design-oriented models (e.g. [32–47]) have been proposed. The calculation procedure in analysis-oriented models consists of two phases: a) by using a lateral strain-to-axial strain model (dilation model), the axial strain of confined concrete (ε_c) is obtained at a given FRP hoop strain (ε_h) and the corresponding FRP confining pressure ($f_{l,f} = K_L\varepsilon_h$); b) by using a stress-strain base model (developed exclusively for axially-loaded concrete subjected to active confinement pressure, $f_{l,active}$), the axial compressive stress (f_c) applied on the FRP-confined concrete corresponding to ε_c is obtained. It should be noted that the important differences in improvements induced by active ($f_{l,active}$) and passive ($f_{l,f}$) confining systems in terms of the axial response of FRP-confined concrete are generally reflected in the failure surface function (the peak stage-related information of the stress-strain model) (Shayanfar *et al.* [45]). Moreover, the key components of an analysis-oriented model (lateral strain-to-axial strain model, stress-strain base model, and failure surface function) require calibration with relevant test results. Even though analysis-oriented models provide a clear interpretation of the confinement mechanism acting on dilation and axial behavior of FRP-confined concrete, they are more time-consuming than what is expected for a design guideline. Design-oriented models have a simpler calculation nature since they are based on a closed-form formulation of the stress-strain relationship, whose key components (transition stress and strain, and ultimate stress and strain) are calibrated by using relevant experimental data. A compressive review and assessment of existing confinement models can be found in Ozbakkaloglu *et al.* [48], Huang *et al.* [49], and Liao *et al.* [50].

Despite a significant number of design-oriented models in the literature, the applicability of the most of them is limited to FRP-confined concrete with a full strain hardening behavior, which is generally simulated by an ascending parabolic-linear stress-strain relationship. There are few models in the literature (e.g. Teng *et al.* [36], Wei and Wu [37], and Cao *et al.* [38]) applicable to stress–strain curves having a strain softening branch beyond the transition zone (stress reduction response). Nonetheless, these models cannot be used for cases with a stress reduction-recovery behavior. Additionally, the reliability of a predictive model, developed based on regression analysis technique, is dependent strongly on the range and frequency of main variables (i.e. f_{c0}, K_L, and β_b) covered by its relevant database. Therefore, for specimens whose main variables are out of the range the model was calibrated, its applicability on the simulation of these specimens is extremely arguable.

Based on the above discussion, this study aims to develop a new confinement model with following features: i) applicable to the cases with a stress reduction-recovery behavior, ii) the main variables be calibrated with a test database of NSC/HSC/UHSC with sufficient/insufficient confinement stiffness, and iii) has a simple design procedure.

In this paper, first, by adopting a FRP confinement stiffness-based index, an FRP-confined concrete's axial response is quantitatively categorized into two groups that have (Fig. 1): i) full strain hardening behavior (Type A), and ii) a stress reduction-recovery behavior (Type B). A new simplified stress-strain expression is proposed to predict the first parabolic branch of both Type A and Type B. Based on a preliminary sensitivity analysis performed on 479 test specimens of Type A, a new formulation is suggested to obtain the gradient of the linear hardening function. By introducing a new methodology, a simplified linear expression is developed to simulate the strain-softening behavior of Type B, which is calibrated using 106 test data. By generating numerical data from the model suggested by Lam and Teng [34], new formulations are also derived for the calculation of the transition zone-related information, through regression analysis technique. With these considerations, the proposed constitutive model, having a simple calculation process, is able to obtain the experimental data of both Type A and Type B with suitable precision. Through a comparative assessment, the superior predictive performance of this model over existing ones selected from the literature is demonstrated.

2. Proposed stress-strain model

Based on experimental results obtained from axial compressive tests executed on FRP-confined circular cross-section concrete specimens (e.g. Ozbakkaloglu and Akin [12], Vincent and Ozbakkaloglu [25], Demir *et al.* [26], Zeng *et al.* [11], Liao *et al.* [27], Wang *et al.* [51], and Li *et al.* [52]), their axial behavior can be categorized as: i) Type A, having a full strain hardening response (Fig. 2a), and ii) Type B, having a stress reduction-recovery behavior (Fig. 2b). In Fig. 2, E_{sh} and E_{ss} represent the gradients of the ascending linear hardening branch, and descending linear softening branch, respectively.

To categorize quantitatively axially-loaded FRP-confined concrete

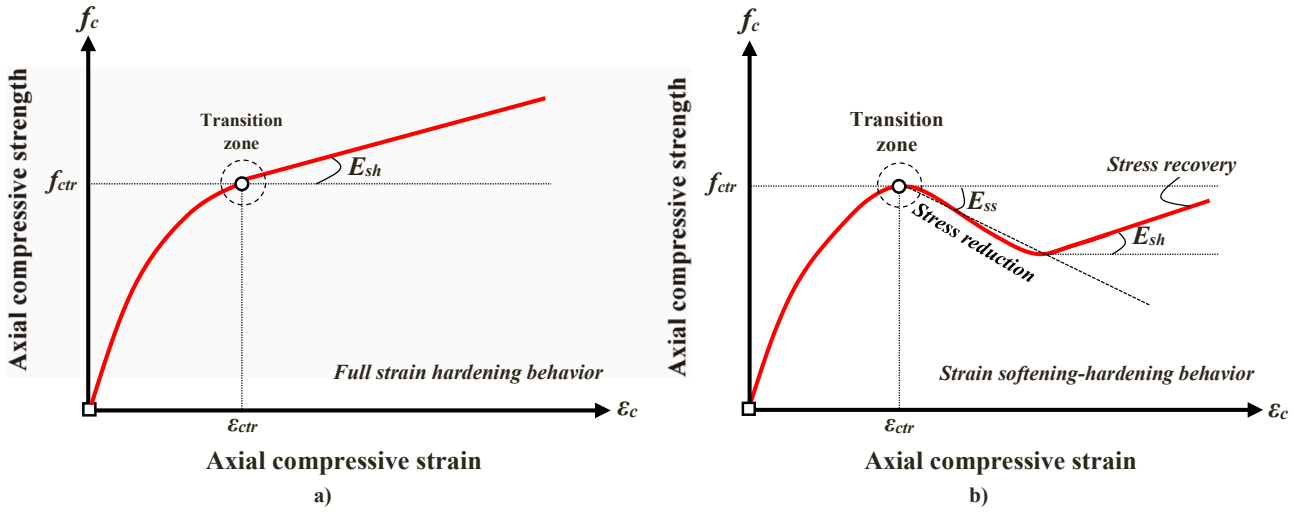


Fig. 2. Stress-strain curve of axially-loaded FRP-confined concrete: a) Type A and b) Type B.

featuring Type A and Type B, Shayanfar *et al.* [53] have recently recommended a non-dimensional FRP confinement stiffness-based threshold (*RI*). Accordingly, for cases with $RI \geq 1$, FRP-confined concrete's response can be considered Type A, otherwise ($RI < 1$) it is of Type B involving a stress reduction-recovery behavior. *RI*can be determined by:

$$RI = \frac{\rho_K}{6 \times 10^{-5} \alpha_b f_{c0}^{\ 1.5}} \tag{1}$$

in which

$$\rho_K = \frac{K_L \varepsilon_{c0}}{f_{c0}} \tag{2}$$

$$K_L = \frac{2 n_f t_f E_f}{b} \tag{3}$$

$$\varepsilon_{c0} = 0.0011 \left(f_{c0}/\beta_L\right)^{0.25} \tag{4}$$

$$0.9 \leq \alpha_b = \sqrt{\beta_b} \leq 1.5 \tag{5}$$

where ρ_K is the normalized FRP confinement stiffness ratio; ε_{c0} is the axial strain corresponding to f_{c0}, which was adopted from Shayanfar *et al.* [54]; n_f is the number of the FRP layers; t_f is the thickness of an FRP layer; E_f is the elastic modulus of FRP layer; b is the cross-section dimension of the column's element; β_L is the column aspect ratio ($\beta_L = L/b$ where L is the column height); and β_b is the normalized column dimension ($\beta_b = b/150$).

It should be noted that besides FRP confinement stiffness, concrete compressive strength and column dimension size involved in Eq. (1), experimental studies [10,17,55] evidenced that the deformability of the FRP confining system is also an effective parameter in the formation of stress reduction-recovery behavior. Depending on FRP confinement stiffness, concrete columns with a highly deformable confining system of Polytheylene naphthalate (PEN) or polyethylene terephthalate (PET) FRP jacket with a very large rupture strain (around 8 %) is more pronounced to exhibit a full stress recovery, compared to conventional FRPs. It is mainly due to the significant activation of the PEN/PET FRP confinement system during a relatively large strain softening phase generating an abrupt concrete expansion, where the activated confinement can recover the stress loss beyond the transition zone. However, the focus of the current study was given on concrete columns confined by conventional FRPs with a linear tensile stress-strain behavior, unlike the bilinear one of PEN/PET FRP.

For the development of the proposed stress-strain model for FRP-confined concrete with/without a stress reduction-recovery behavior, in the present study, the following assumptions were taken (Fig. 2):

i) Stress–strain responses ($f_c - \varepsilon_c$) of both Type A and Type B have the same genesis up to the transition zone, and can be formulated by adopting a parabolic function.
ii) Transition zone-related information (ε_{ctr} and f_{ctr}) has the same nature for both Type A and Type B.
iii) For cases with $RI < 1$, the stress reduction and stress recovery phases of $f_c - \varepsilon_c$ relationship beyond the transition zone can be formulated by adopting descending and ascending linear functions, respectively.
iv) For cases with $RI \geq 1$, the strain hardening portion of the $f_c - \varepsilon_c$ relationship beyond the transition zone can be formulated by adopting a linear function.
v) The gradient of the ascending linear stress-stress function is assumed as E_{sh} for the both Type A and Type B columns.

It is noteworthy that a reliable stress-strain model should have a unified nature with respect to *RI* index. Accordingly, predictions obtained from this unified model are smoothly converted from $RI < 1$ (Type B) to $RI \geq 1$ (Type A), without any discontinuity caused by the type of stress-strain behavior. Likewise, the developed model was tailored for being applied based on the concrete compressive strength (f_{c0}), without any discontinuity imposed due to concrete classes (i.e. NSC, HSC and UHSC). Accordingly, instead of developing separate models for each concrete class, in this study, a single stress-strain model generalized for various strength classes was proposed. For this purpose, the key components of the proposed model (e.g. the gradients of the strain-hardening and -softening portions) were calibrated using a database covering NSC, HSC and UHSC columns.

3. Stress-strain relation up to the transition point for Type A and Type B responses

Based on experimental observations, the initial $f_c - \varepsilon_c$ of FRP-confined concrete up to the transition point (ε_{ctr} and f_{ctr}) was assumed as a polynomial function with the degree of n_{d1}:

$$\frac{f_c}{f_{ctr}} = A_1 \left(\frac{\varepsilon_c}{\varepsilon_{ctr}}\right)^{n_{d1}} + A_2 \left(\frac{\varepsilon_c}{\varepsilon_{ctr}}\right) + A_3 \text{ for } \varepsilon_c \leq \varepsilon_{ctr} \tag{6}$$

where A_1 to A_3 are the constant coefficients of the function. The boundary conditions to derive these constant coefficients can be considered as follows:

$$i)\varepsilon_c/\varepsilon_{ctr}=0\rightarrow f_c/f_{ctr}=0 \tag{7a}$$

$$ii)\varepsilon_c/\varepsilon_{ctr}=1\rightarrow f_c/f_{ctr}=1 \tag{7b}$$

$$iii)\varepsilon_c/\varepsilon_{ctr}=1\rightarrow df_c/d\varepsilon_c=E_{sh} \tag{7c}$$

Using Eq. (7), Eq. (6) yields:

$$\frac{f_c}{f_{ctr}}=\left[\frac{1-E_{sh}/E_{ctr}}{1-n_{d1}}\right]\left(\frac{\varepsilon_c}{\varepsilon_{ctr}}\right)^{n_{d1}}+\left[\frac{E_{sh}}{E_{ctr}}-\frac{n_{d1}}{1-n_{d1}}\left(1-\frac{E_{sh}}{E_{ctr}}\right)\right]\left(\frac{\varepsilon_c}{\varepsilon_{ctr}}\right) \tag{8}$$

in which

$$E_{ctr}=\frac{f_{ctr}}{\varepsilon_{ctr}} \tag{9}$$

Based on the experimental data of n_{d1} obtained from 191 test specimens of FRP-confined concrete, in this study, n_{d1} was considered equal to 2.5, whose good predictive performance can be seen in Fig. 3a. Accordingly, by $n_{d1}=2.5$, Eq. (8) can be rearranged as:

$$\frac{f_c}{f_{ctr}}=-\frac{2}{3}\left[1-\frac{E_{sh}}{E_{ctr}}\right]\left(\frac{\varepsilon_c}{\varepsilon_{ctr}}\right)^{2.5}+\frac{2}{3}\left[\frac{5}{2}-\frac{E_{sh}}{E_{ctr}}\right]\left(\frac{\varepsilon_c}{\varepsilon_{ctr}}\right) \tag{10}$$

Furthermore, for the implementation of a further simplification, a set of numerical data of E_{sh}/E_{ctr} was generated, where the formulations used for the calculation of E_{sh} and E_{ctr} will be addressed in the sections of 3.2 and 5, respectively. Accordingly, the average value of E_{sh}/E_{ctr} was assumed equal to 0.14, whose good predictive performance is shown in Fig. 3b. Hence, by putting $E_{sh}/E_{ctr}=0.14$ in Eq. (10), the initial $f_c-\varepsilon_c$ of FRP-confined concrete can be determined as:

$$f_c=\left[-0.57\left(\frac{\varepsilon_c}{\varepsilon_{ctr}}\right)^{2.5}+1.57\left(\frac{\varepsilon_c}{\varepsilon_{ctr}}\right)\right]f_{ctr}\ for\ \varepsilon_c\le\varepsilon_{ctr} \tag{11}$$

This equation offers a simple formulation for the calculation of $f_c-\varepsilon_c$ relation of axially-loaded FRP-confined concrete.

4. Stress-strain relation of the linear hardening branch (Type A)

For the case of Type A columns, the $f_c-\varepsilon_c$ relation beyond the transition zone can be formulated by considering a linear equation:

$$f_c=f_{ctr}+E_{sh}(\varepsilon_c-\varepsilon_{ctr})\ for\ \varepsilon_c\ge\varepsilon_{ctr} \tag{12}$$

where E_{sh} is the gradient of the linear function. Based on a preliminary sensitivity analysis, performed on 479 test data of FRP-confined concrete specimens, f_{c0} and K_L were evidenced as the most significant parameters influencing E_{sh}, whereas β_b and E_f have less influence, as presented in Fig. 4.

Accordingly, based on non-linear regression analysis, a new formulation was developed to calculate E_{sh} as a function of f_{c0} and K_L:

$$E_{sh}=12.5{K_L}^{0.47}{f_{c0}}^{0.44} \tag{13}$$

Fig. 5a examines the performance of Eq. (13). As can be seen, there is a good agreement between analytical and experimental results. Introducing Eq. (13) into Eq. (12) results in:

$$f_c=f_{ctr}+12.5{K_L}^{0.47}{f_{c0}}^{0.44}(\varepsilon_c-\varepsilon_{ctr})\ for\ \varepsilon_c\ge\varepsilon_{ctr} \tag{14}$$

where Eq. (14) has a simple format for the calculation of $f_c-\varepsilon_c$ relation of FRP-confined concrete with a full strain hardening behavior.

For a further examination of the predictive accuracy of Eq. (13), its performance is compared with that of existing formulations developed by Samaan et al. [56], Teng et al. [36], Wei and Wu [37], Cao et al. [38], Lin et al. [57], ACI 440.2R-17 [58], Fallahpour et al. [39], *fib* [59] and Shayanfar *et al.* [53]. As can be seen in Fig. 5 and Table 1, Teng *et al.* [36] provides the most accurate prediction of E_{sh} amongst the considered existing models. Nonetheless, based on the obtained statistical indicators, the proposed model has a superior predictive performance over all these models. It should be noted that in existing models, E_{sh} is generally expressed as $E_{sh}=(f_{cu}-f_{c0})/\varepsilon_{cu}$, or $E_{sh}=(f_{cu}-f_{ctr})/(\varepsilon_{cu}-\varepsilon_{ctr})$, where f_{cu} and ε_{cu} are ultimate axial stress and strain of an axially-loaded FRP-confined concrete. However, besides accurate predictions, the proposed formulation of Eq. (13) offers a simpler calculation procedure, which is a suitable characteristic for the design practice.

5. Post-peak strain softening-hardening behavior (Type B)

Based on experimental observations (Ozbakkaloglu and Akin [12], Vincent and Ozbakkaloglu [25], and Zeng et al. [17]), the axial response of Type B columns beyond the transition strain ($\varepsilon_c>\varepsilon_{ctr}$) was assumed to have two branches: a descending ${f_c}^{II}-\varepsilon_c$ and an ascending ${f_c}^{III}-\varepsilon_c$, as shown in Fig. 6. Accordingly, at a given ε_c, f_c can be calculated as the maximum of these branches:

$$f_c=\max\left[{f_c}^{II},{f_c}^{III}\right] \tag{15}$$

whose components will be addressed in the following sections.

5.1. Determination of ${f_c}^{II}-\varepsilon_c$

In this study, the descending ${f_c}^{II}-\varepsilon_c$ was formulated by a linear function from the transition zone to a constant stress plateau, hereafter

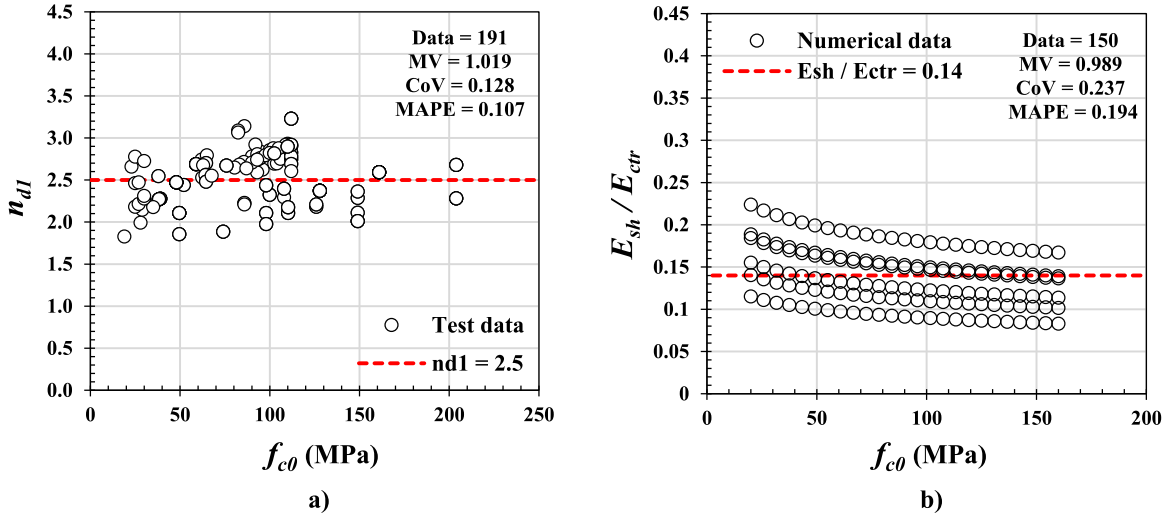


Fig. 3. Variations of n_{d1} and E_{sh}/E_{ctr} with f_{c0}. **Note:** MV = Mean Value; CoV = Coefficient of Variation; MAPE = Mean Absolute Percentage Error.

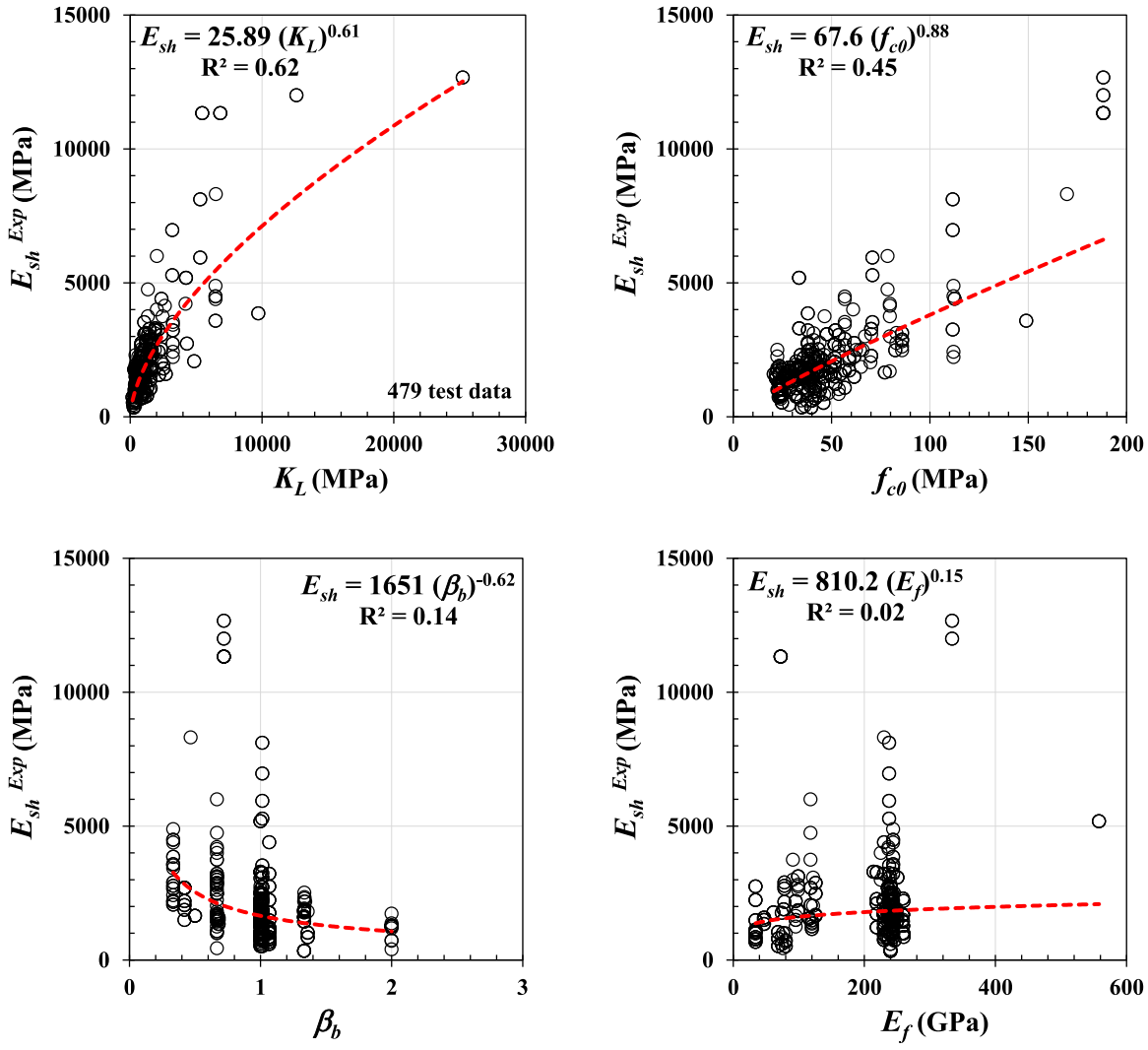


Fig. 4. Degree dominance of K_L, f_{c0}, β_b and E_f variables in E_{sh}.

designated by the minimum capacity ($f_{c,\,\min}$), as shown in Fig. 6. Accordingly, the $f_c^{\,II} - \varepsilon_c$ is proposed as:

$$f_c^{\,II} = f_{ctr} + E_{ss}(\varepsilon_c - \varepsilon_{ctr}) \text{ for } \varepsilon_c \geq \varepsilon_{ctr} \tag{16}$$

where E_{ss} is the softening gradient of the linear function. A new formulation was developed to determine E_{ss} where it was assumed:

$$E_{ss} = \frac{f_{ci} - f_{ctr}}{\varepsilon_{ci} - \varepsilon_{ctr}} \tag{17}$$

in which ε_{ci} is the axial strain corresponds to an axial stress (f_{ci}) at half of the difference ($\Delta_c = f_{ctr} - f_{c,\,\min}$) of the transition stress and minimum capacity, as illustrated in Fig. 6. Accordingly, f_{ci} corresponding to ε_{ci} can be written as:

$$f_{ci} = f_{ctr} - 0.5\Delta_c = f_{ctr} - 0.5\left(f_{ctr} - f_{c,\,\min}\right) \tag{18}$$

By assuming $f_{c,\,\min} = f_{ctr} - 0.85f_{c0}$ (Shayanfar *et al.* [53]), Eq. (18) can be rearranged as:

$$f_{ci} = f_{ctr} - 0.5\left(f_{ctr} - f_{ctr} + 0.85f_{c0}\right) = f_{ctr} - 0.425f_{c0} \tag{19}$$

By introducing Eq. (19) into Eq. (17), E_{ss}can be derived as:

$$E_{ss} = \frac{\left(f_{ctr} - 0.425f_{c0}\right) - f_{ctr}}{\varepsilon_{ci} - \varepsilon_{ctr}} = -\frac{0.425f_{c0}}{\varepsilon_{ci} - \varepsilon_{ctr}} \tag{20}$$

Replacing Eq. (20) into Eq. (17) results in

$$f_c^{\,II} = f_{ctr} - \frac{0.425f_{c0}}{\varepsilon_{ci} - \varepsilon_{ctr}}(\varepsilon_c - \varepsilon_{ctr}) \tag{21}$$

By rearranging the above equation gives:

$$f_c^{\,II} = f_{ctr} - 0.425f_{c0}\frac{\varepsilon_c - \varepsilon_{ctr}}{\varepsilon_{ci} - \varepsilon_{ctr}} \tag{22}$$

Therefore, the descending branch of the axial response of Type B columns ($f_c^{\,II} - \varepsilon_c$) can be calculated by Eq. (22). However, for the calculation of this relationship, ε_{ci} must be known. Considering that when RI is almost one ($RI \simeq 1$), E_{ss} tends to be zero ($E_{ss} \simeq 0$) and ε_{ci} to $+\infty$, by which Eq. (22) would be equal to $f_c^{\,II} = f_{ctr}$. However, by decreasing RI from one to almost zero, ε_{ci} should tend to the strain of unconfined concrete (ε_{ci0}) corresponding to $0.5f_{c0}$ (Fig. 6). Based on the above conditions, the following formulation is proposed to determine ε_{ci}:

$$\varepsilon_{ci} = (1 - RI)^{-\eta_\varepsilon}\varepsilon_{ci0} > \varepsilon_{ctr} \text{ for } RI < 1 \tag{23a}$$

$$\varepsilon_{ci} = +\infty \text{ for } RI \geq 1 \tag{23b}$$

where η_ε is the exponent of the function, by which the relationship of ε_{ci} with RI can be calibrated with experimental data. In this study, the Shayanfar *et al.* [38]'s recommendation was used to determine ε_{ci0} which was calibrated based on 217 tests of unconfined concrete specimens:

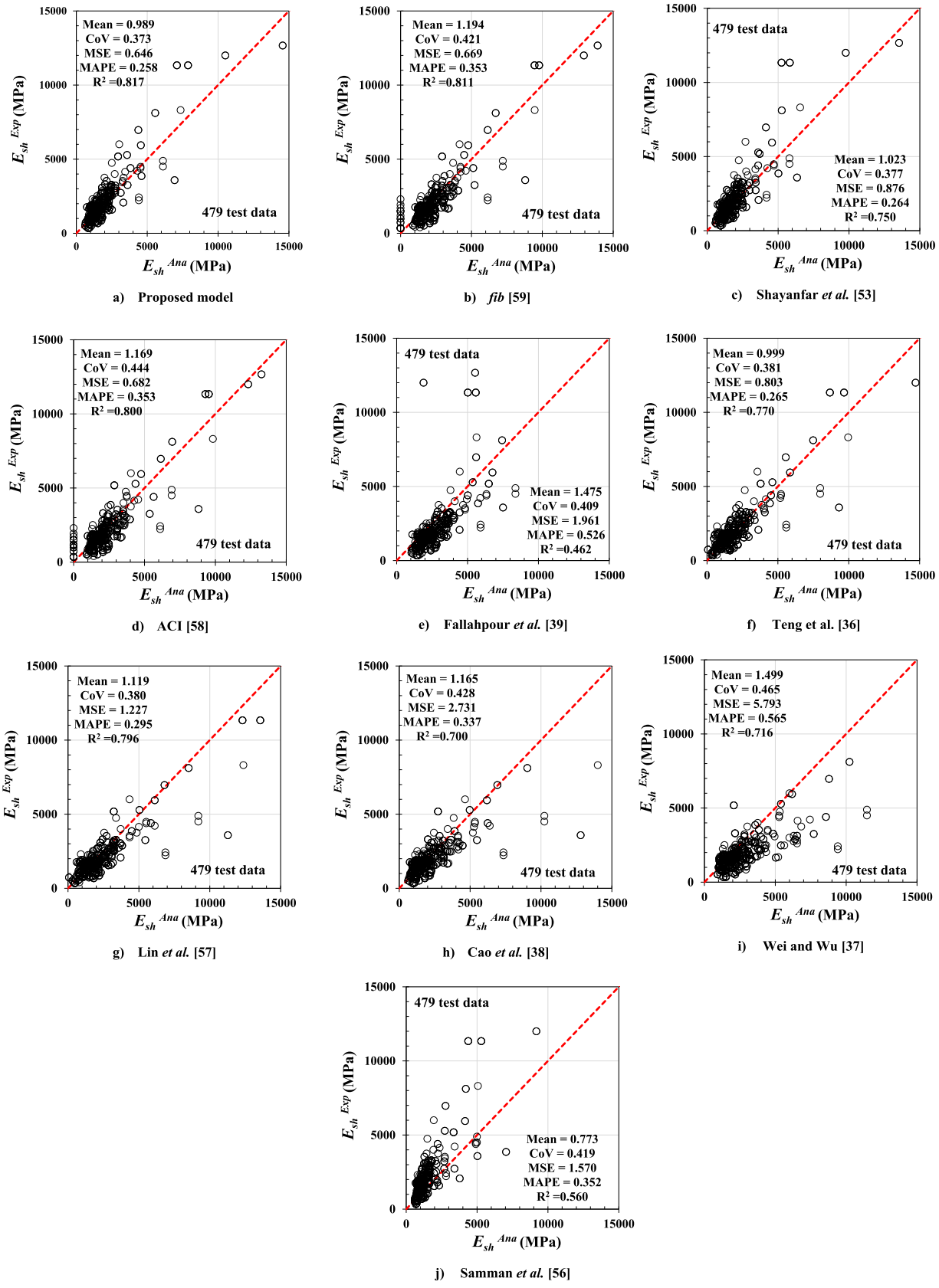


Fig. 5. Experimental versus analytical values of E_{sh}.

Table 1
Statistical assessment of proposed and existing predictive models for E_{sh}.

ID	Test data	MV	CoV	MSE	MAPE	R^2
Proposed model	**479**	**0.989**	**0.373**	**0.646**	**0.258**	**0.817**
fib [59]		1.194	0.421	0.669	0.353	0.811
Shayanfar et al. [53]		1.023	0.377	0.876	0.264	0.750
ACI440.2R−17 [58]		1.169	0.444	0.682	0.353	0.800
Fallahpour et al. [39]		1.475	0.409	1.961	0.526	0.462
Teng et al. [36]		0.999	0.381	0.803	0.265	0.770
Lin et al. [57]		1.119	0.380	1.227	0.295	0.796
Cao et al. [38]		1.165	0.428	2.731	0.337	0.700
Wei and Wu [37]		1.499	0.465	5.793	0.565	0.716
Samaan et al. [56]		0.773	0.419	1.570	0.352	0.560

Note: MV = Mean Value; CoV = Coefficient of Variation; MSE = Mean Squared Error; MAPE = Mean Absolute Percentage Error; R^2 = R-squared

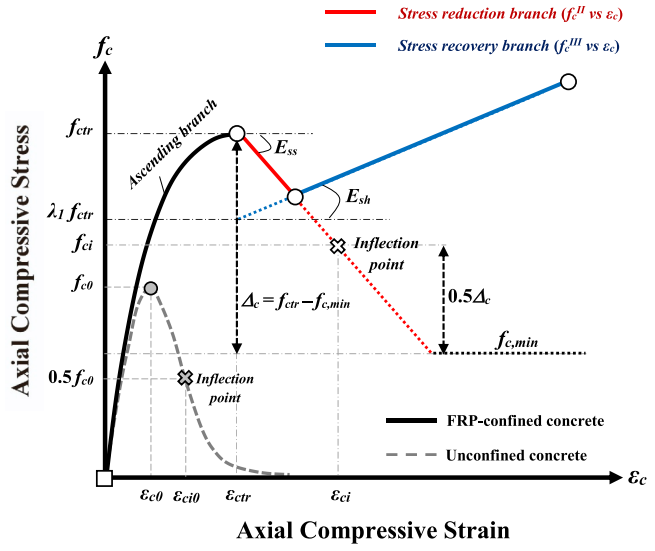


Fig. 6. Assumed stress-strain behavior of Type B columns.

$$\varepsilon_{ci0} = 0.026 f_{c0}^{-0.34} \beta_L^{-0.81} \beta_b^{-0.1} \quad (24)$$

The η_ε exponent was determined through back analysis method using 109 experimental stress-strain curves of Type B. By performing non-linear regression analysis, η_ε was developed as follows:

$$\eta_\varepsilon = 0.01 RI^{-0.55} f_{c0}^{0.93} \beta_b^{-0.4} \quad (25)$$

The performance of Eq. (25) is presented in Fig. 7.

5.2. Determination of $f_c^{III} - \varepsilon_c$

The ascending $f_c^{III} - \varepsilon_c$ (the stress recovery response) was formulated by a linear function, whose slope (E_{sh}) was assumed to have the same nature as that associated with Type A ($E_{sh} = 12.5 K_L^{0.47} f_{c0}^{0.44}$). Accordingly, the $f_c^{III} - \varepsilon_c$ was proposed as:

$$f_c^{III} = \lambda_1 f_{ctr} + 12.5 K_L^{0.47} f_{c0}^{0.44} (\varepsilon_c - \varepsilon_{ctr}) \; for \; \varepsilon_c \geq \varepsilon_{ctr} \quad (26)$$

where λ_1 is a reduction factor, considered to reflect the effect of the stress reduction beyond the transition zone. Considering that there is no strain-softening behavior in the column's response when RI is almost one ($RI \simeq 1$), λ_1 would be equal to one ($\lambda_1 \simeq 1$). By decreasing RI from one to almost zero, λ_1 should also decrease from one to zero corresponding to unconfined concrete ($K_L = 0$) whose axial stress-strain relation does not contain a stress recovery response ($\lambda_1 = 0 \rightarrow f_c^{III} = 0$). Based on the above conditions, the λ_1 can be determined from:

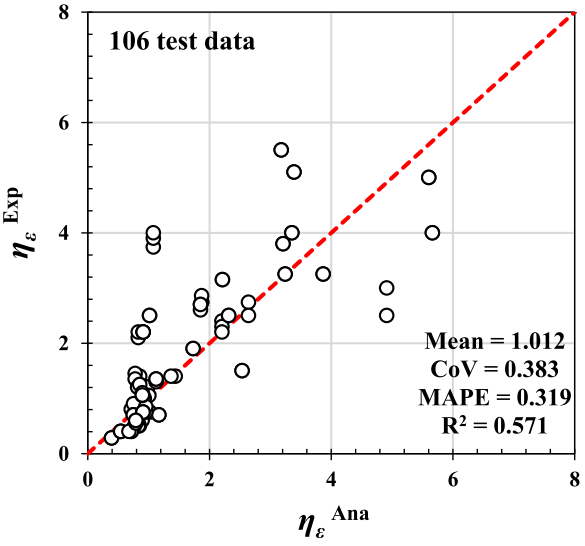


Fig. 7. Performance of Eq. (25).

$$\lambda_1 = RI^{\eta_1} \leq 1 \quad (27)$$

where the η_1 exponent was obtained through non-linear regression analysis using 98 experimental stress-strain curves of Type B, having resulted:

$$\eta_1 = 0.23 RI^{0.6} f_{c0}^{0.3} \beta_b \quad (28)$$

The performance of this equation is presented in Fig. 8 by comparing to the corresponding experimental values, η_1^{Exp}.

6. Transition zone-related information

For the calculation of $f_c - \varepsilon_c$ behavior of Type A and Type B columns, the information regarding the transition stress and strain is required to be addressed, as input parameters. For the determination of the transition strain (ε_{ctr}), Lam and Teng [34] proposed the following equation:

$$\frac{\varepsilon_{ctr}}{\varepsilon_{c0}} = \frac{2 f_{c0}}{(E_c - E_{sh}) \varepsilon_{c0}} \quad (29)$$

where E_c is the concrete modulus elasticity, which was assumed as $E_c =$

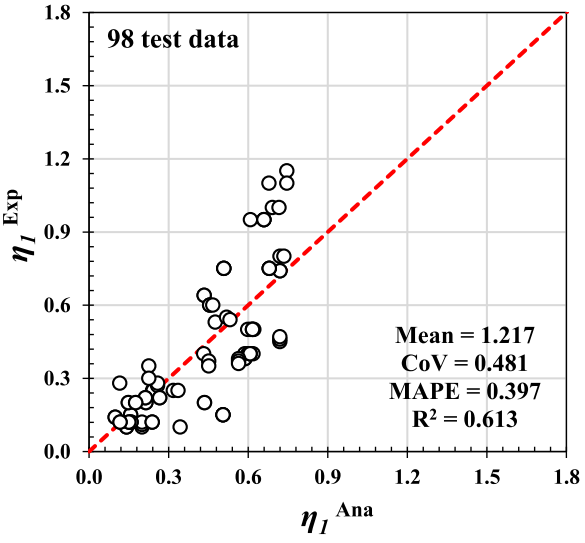


Fig. 8. Performance of Eq. (28).

$4730\sqrt{f_{c0}}$ ([58]). By introducing Eq. (4) and (13) into Eq. (29) results:

$$\frac{\varepsilon_{ctr}}{\varepsilon_{c0}} = \frac{2f_{c0}}{0.0011\left(\frac{f_{c0}}{\beta_L}\right)^{0.25}\left(4730\sqrt{f_{c0}} - 12.5{K_L}^{0.47}{f_{c0}}^{0.44}\right)} \quad (30)$$

Based on a sensitivity analysis, performed on the numerical data generated by Eq. (30), f_{c0} was found to have the most significant influence on $\varepsilon_{ctr}/\varepsilon_{c0}$. Considering this aspect and executing non-linear regression analysis, Eq. (30) was reduced to the following one:

$$\frac{\varepsilon_{ctr}}{\varepsilon_{c0}} = 0.4{f_{c0}}^{0.25}{K_L}^{0.025} \geq 1 \quad (31)$$

in which the term ${K_L}^{0.025}$ unifies the formulation for FRP-confined concrete and unconfined concrete columns. As Fig. 9a shows, there is a close agreement between results obtained from Eqs. (30) and (31).

On the other hand, based on the stress-strain function suggested by Lam and Teng [34] for the prediction of the strain-hardening portion of FRP-confined concrete's behavior beyond the transition zone, the axial stress (f_c) for a given axial strain (ε_c) can be calculated by:

$$f_c = f_{c0} + E_{sh}\varepsilon_c \quad (32)$$

Accordingly, in the case that $f_c = f_{ctr}$ corresponding to $\varepsilon_c = \varepsilon_{ctr}$, Eq. (32) can be written as:

$$f_{ctr} = f_{c0} + E_{sh}\varepsilon_{ctr} \quad (33)$$

Introducing Eqs. (4), (13), and (31) into Eq. (33) leads to:

$$f_{ctr} = f_{c0} + 0.0055{K_L}^{0.495}{f_{c0}}^{0.94}{\beta_L}^{-0.25} \quad (34)$$

Normalizing the above equation by f_{c0} results in:

$$\frac{f_{ctr}}{f_{c0}} = 1 + 0.0055{K_L}^{0.495}{f_{c0}}^{-0.06}{\beta_L}^{-0.25} \quad (35)$$

Based on a sensitivity analysis performed on the numerical data generated by Eq. (35), it was found the normalized f_{ctr}/f_{c0} is significantly dependent on K_L, whereas f_{c0} and β_L have much less impact. Considering this fact and executing a non-linear regression analysis, Eq. (35) was resumed to:

$$\frac{f_{ctr}}{f_{c0}} = 0.8{K_L}^{0.05} \geq 1 \quad (36)$$

whose suitable predictive performance is shown in Fig. 9b.

For a further examination, the predictive performance of Eq. (36) was also evaluated with 99 experimental data of f_{ctr} available in the literature, as presented in Fig. 10. As can be seen, Eq. (36) is able to provide a close prediction of the experimental counterparts.

7. Calculation procedure

For the determination of f_c *vs* ε_c relationship of FRP-confined concrete based on the proposed stress-strain model, the following steps can be followed (Fig. 11):

1. Calculate ε_{ctr} and f_{ctr} by Eqs. (36) and (31)
2. Calculate *RI* by Eq. (1)

   For Type *A columns* ($RI \geq 1$)
3. Calculate f_c *vs* ε_c relation by Eqs. (11) and (14)

   For Type *B columns* ($RI \leq 1$)
5. Calculate ε_{ci} and λ_1 by Eqs. (23) and (27)
6. Calculate f_c^{II} and f_c^{III} by Eq. (22) and (26)
7. Calculate f_c *vs* ε_c relation by Eqs. (11) and (15)

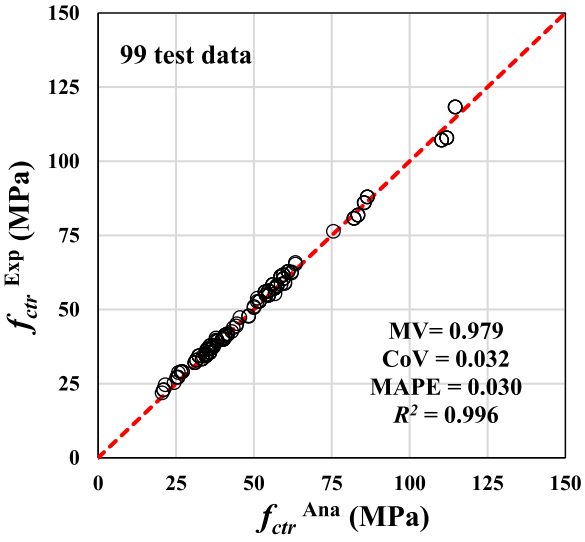


Fig. 10. Performance of Eq. (36).

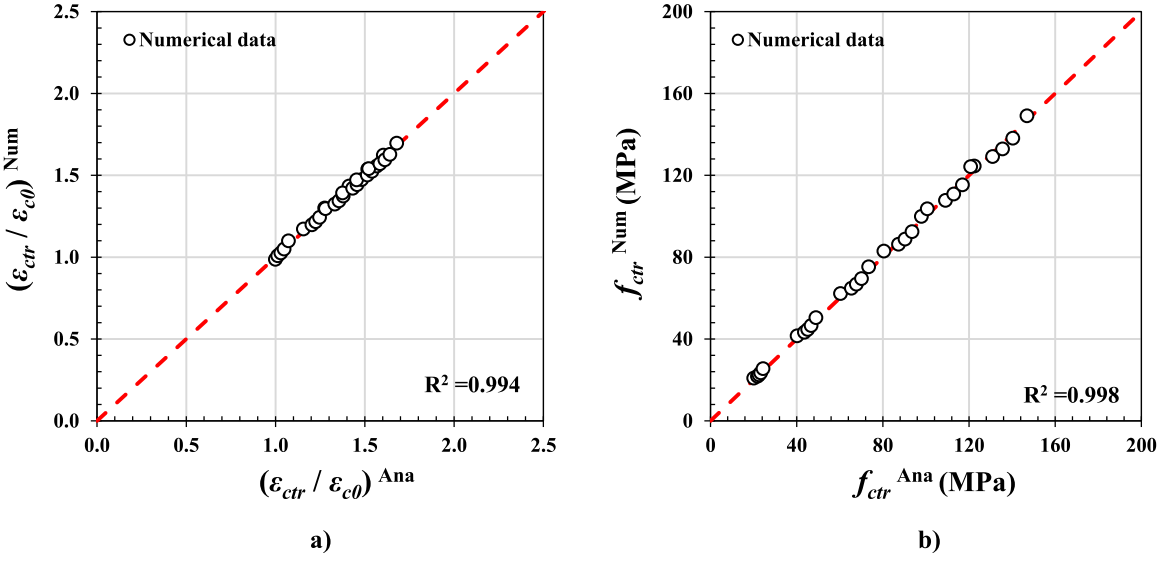


Fig. 9. Transition zone-related information: a) transition strain, b) transition stress.

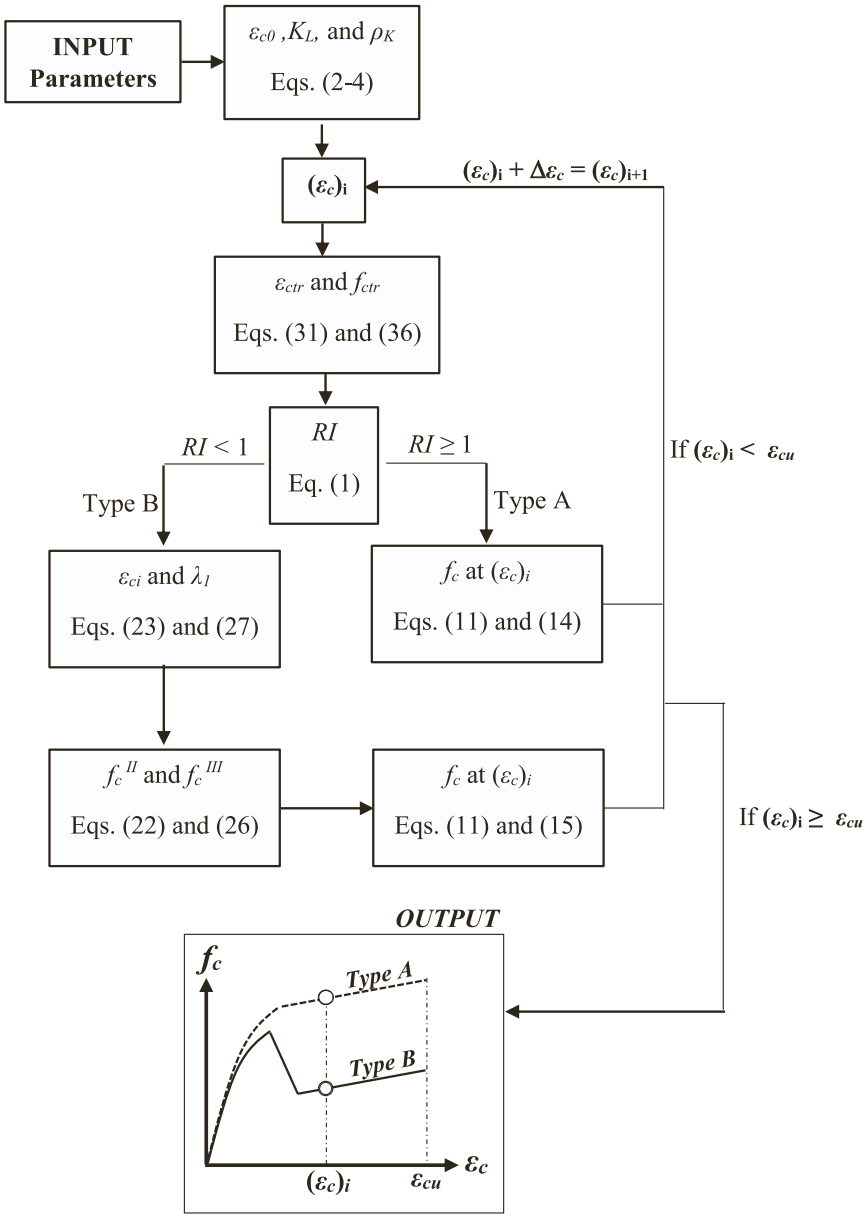


Fig. 11. Flowchart for the calculation process of the stress-strain behavior of Type A and Type B columns.

As can be seen, the proposed model provides a simple calculation process for FRP-confined concrete with/without a stress reduction-recovery behavior (Type A and Type B).

For a clear description of this calculation process, two detailed examples regarding the application of the proposed stress-strain model for the prediction of the axial response of FRP-confined concrete specimens of Type A and Type B are presented in Appendixes B and C, respectively.

It is noteworthy that several formulations are available in the literature (e.g. [34–41,57–59]) for the estimation of the ultimate condition of circular cross-section columns confined by FRP jacket. However, in the current study, the exact values of the ultimate axial strain (ε_{cu}) obtained from the experiments were used to terminate the calculation process (Fig. 11), since the main focus of this study was on the development of a versatile design-oriented model to calculate the complete stress-strain relationship containing a stress reduction-recovery behavior.

8. Verification of the proposed model

Even though the key components of the proposed model were calibrated using experimental data, its capability in terms of the prediction of the complete stress-strain relationship needs demonstration. For this purpose, the stress-strain behavior of 30 experimental axially-loaded FRP-confined concrete specimens with/without a stress reduction-recovery behavior is predicted by using the proposed model. For having a more comprehensive comparative evaluation, this model's performance is compared to that of existing stress-strain models proposed by Teng *et al.* [36], Wei and Wu [37], Cao *et al.* [38], ACI 440.2R-17 [42], Fallahpour et al. [39] and *fib* [59].

For Type A columns, Fig. 12 compares the stress-strain curves of axially-loaded FRP-confined concrete specimens obtained from the analytical confinement models and experiments conducted by Barros and Ferreira [11], Eid *et al.* [19], Ozbakkaloglu and Akin [12], Wang *et al.* [60], Vincent and Ozbakkaloglu [25], Ozbakkaloglu and Vincent [14], De Oliveira *et al.* [3], and Lin *et al.* [4]. As shown, the proposed model could provide a close prediction of experimental counterparts of

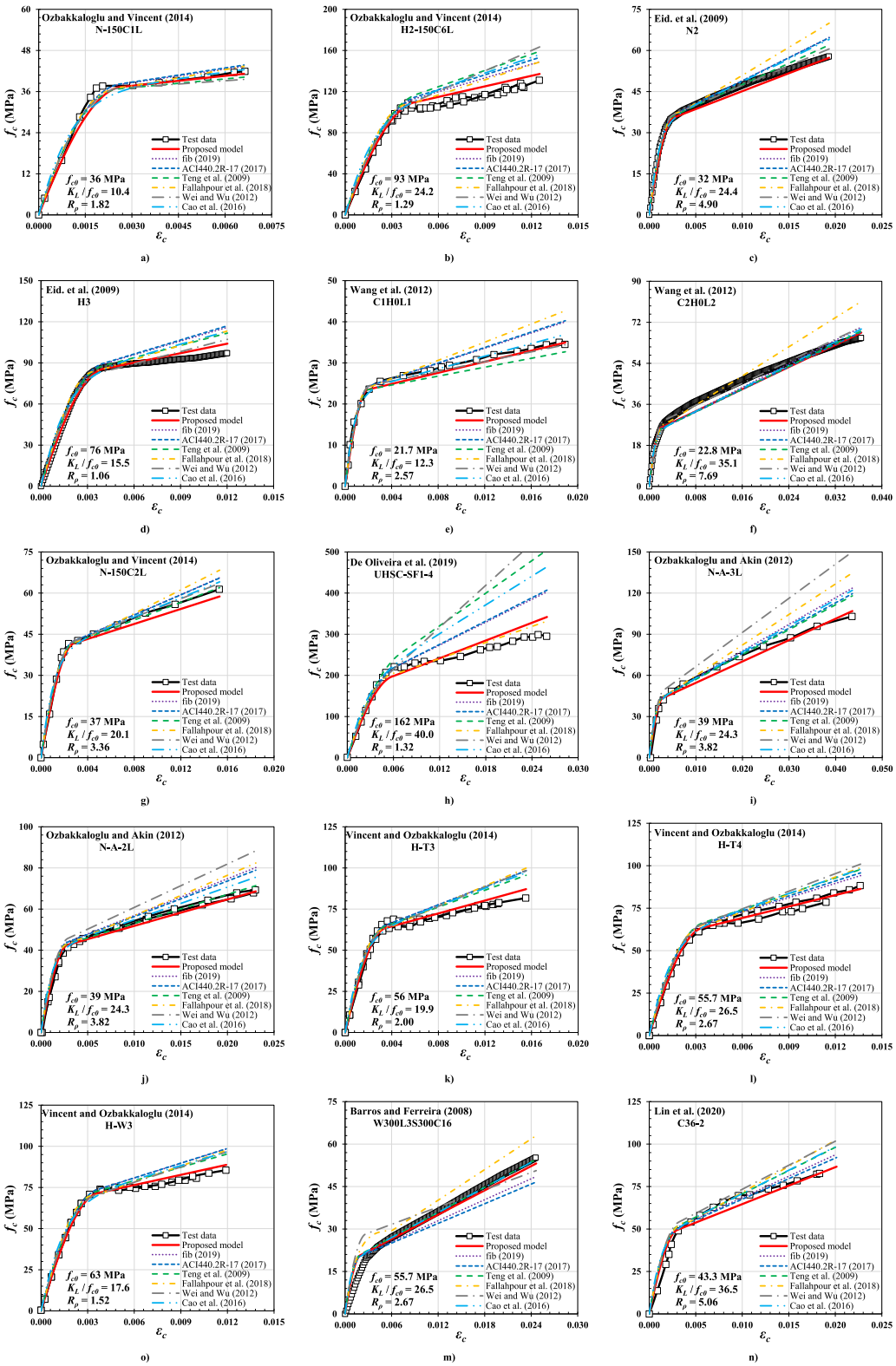


Fig. 12. Stress-strain curves of axially-loaded FRP-confined concrete specimens obtained from the analytical models and experiments conducted by Barros and Ferreira [11], Eid et al. [19], Ozbakkaloglu and Akin [12], Wang et al. [60], Vincent and Ozbakkaloglu [25], Ozbakkaloglu and Vincent [14], De Oliveira et al. [3], and Lin et al. [4].

Type A. Moreover, compared to the existing stress-strain models, the superior predictive performance of the proposed model can be verified.

For Type B columns, in Fig. 13, the stress-strain curves of axially-loaded FRP-confined concrete specimens obtained from the analytical models and experiments conducted by Eid et al. [19], Ozbakkaloglu and Akin [12], Vincent and Ozbakkaloglu [25], Ozbakkaloglu and Vincent [14], Lim and Ozbakkaloglu [2], and De Oliveira et al. [3] are compared. For this case, the proposed model could demonstrate a suitable performance in the simulation of experimental counterparts with a stress reduction-recovery behavior. Furthermore, the superior performance of

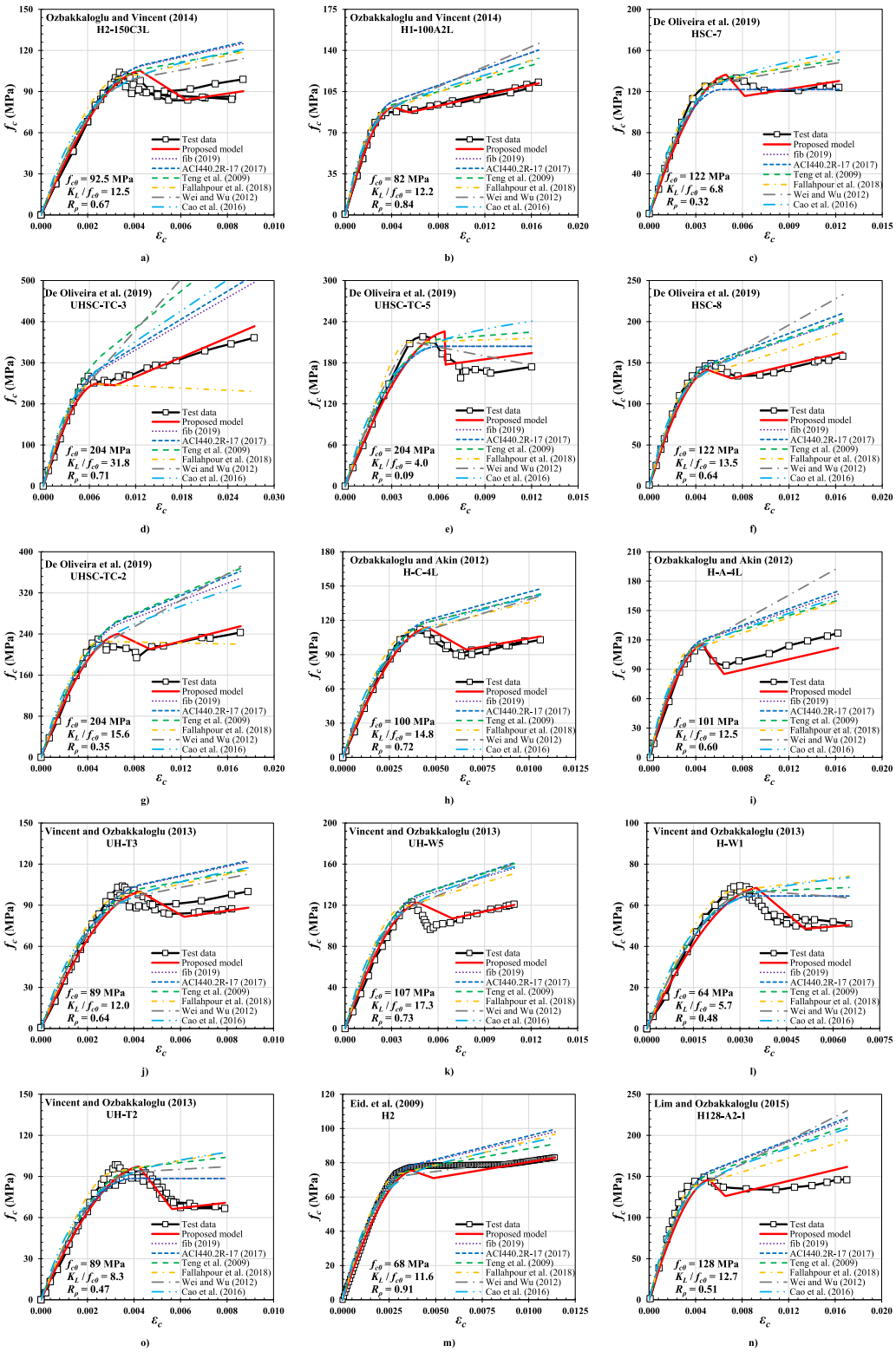


Fig. 13. Stress-strain curves of axially-loaded FRP-confined concrete specimens obtained from the analytical models and experiments conducted by Eid et al. [19], Ozbakkaloglu and Akin [12], Vincent and Ozbakkaloglu [25], Ozbakkaloglu and Vincent [14], Lim and Ozbakkaloglu [2], and De Oliveira et al. [3].

the proposed model over the considered models can be verified for the case of Type B columns, where these last ones provided non-conservative predictions.

9. Limitations of the proposed model

The applicability of the proposed model is limited to circular cross-section columns confined by FRP jacket. Besides FRP confinement stiffness, concrete compressive strength, and column dimension size, which are involved in Eq. (1), experimental studies [61–64] evidenced

that non-circularity of the column's cross-section is an effective parameter in the formation of stress reduction-recovery behavior. This is remarkably pronounced for lightly-confined non-circular cross-section columns with sharp edges and a large sectional aspect ratio. Accordingly, it is recommended to extend the applicability of Eq. (1) by considering the effect of corner radius ratio and sectional aspect ratio. Furthermore, the key components of the proposed stress-strain models (i.e. the transition zone-related information and the gradients of the strain-hardening and -softening portions) must be recalibrated by considering the non-circularity effects.

The proposed model is applicable only to axially-loaded unreinforced concrete columns. It is well-established that the enhancements generated by the FRP lateral confinement system on the axial and dilation behavior of unreinforced concrete columns would noticeably differ from those in the case of RC columns with a combined confinement provided by transverse steel reinforcement and FRP wraps, dependent on their confinement stiffness levels [60]. Based on Lin *et al.* [57] and Shayanfar *et al.* [65], the transition zone-related information (f_{ctr} and ε_{ctr}) in the stress-strain relation of FRP-confined RC columns is strongly dependent on the confinement stiffness ratio between steel and FRP. The gradient of the strain-hardening linear portion (E_{sh}) is also influenced by considering the impact of steel transverse reinforcement. Accordingly, to extend the applicability of the proposed model to FRP-confined RC columns, the formulations developed forf_{ctr} and ε_{ctr} must be revised by taking into account the confinement stiffness ratio between FRP and steel reinforcement. An incremental factor also needs to be considered in term of E_{sh} to reflect the influence of steel reinforcement.

Even though the test database used for the calibration of the proposed model covers a relatively wide-range of column dimension size in the range of 50–326 mm, the majority of involved data concerns the small prototypes, considering the mean and coefficient of variation (CoV) are 138 mm and 0.335, respectively. Hence, the validation of the proposed model for large-scale FRP-confined concrete still requires further demonstration. Once an adequate number of test results of large-scale specimens is available, a recalibration approach can be applied to the model's key components.

It should be noted that despite a proper balance between the simplicity of the calculation process and the accuracy of stress-strain prediction, the proposed design-oriented model should not be directly implemented in practical design, as a ready-made solution. For the assured application of the model in real strengthening cases, besides recalibrating its key components based on large-scale test specimens, relevant safety factors should be determined due to uncertainties in terms of geometrical parameters and the mechanical properties of FRP confinement and concrete, as well as their interactions.

10. Summary and conclusions

This study has presented a new unified design-oriented model for predicting the stress-strain behavior of axially-loaded FRP-confined normal/high/ultrahigh-strength concrete columns of circular cross-section. First, by adopting an FRP confinement stiffness-based index, an FRP-confined concrete's axial response is quantitatively categorized into two groups that have: i) a full strain-hardening behavior (Type A), and ii) a stress reduction-recovery behavior (Type B). For both cases of Type A and Type B, a simplified stress-strain relation was developed for the first portion of axial behavior prior to the transition zone. Based on a large test database of Type A, a well-calibrated formulation was developed to calculate the slope of hardening linear functions, dependent strongly on concrete strength and confinement stiffness. By introducing a new methodology, a linear function was developed to simulate the strain-softening portion in the stress-stress behavior of Type B, whose gradient was calibrated using a large test database of Type B. Furthermore, based on a reliable numerical database obtained from the models suggested by Lam and Teng [34], simplified formulations are proposed to calculate the stress and strain at the transition zone of the stress-strain relations. With these considerations, the proposed constitutive model, having a simple calculation process, is able to obtain the experimental stress-strain behavior of both Type A and Type B with suitable precision. Through comparative assessment with existing models and guidance, the superior predictive performance of this model over existing ones selected from the literature is demonstrated.

CRediT authorship contribution statement

Javad Shayanfar: Writing – original draft, Validation, Methodology, Investigation, Formal analysis, Data curation. **João P. C. Pereira:** Writing – review & editing, Validation, Investigation, Data curation. **Joaquim A. O. Barros:** Writing – review & editing, Supervision, Methodology, Funding acquisition, Conceptualization.

Declaration of Competing Interest

The authors declare that they have no known competing financial interests or personal relationships that could have appeared to influence the work reported in this paper.

Data availability

Data will be made available on request.

Acknowledgments

This study is a part of the project "Sticker –Innovative technique for the structural strengthening based on using CFRP laminates with multifunctional attributes and applied with advanced cement adhesives", with the reference POCI-01-0247-FEDER-039755. The first author also acknowledges the support provided by the project 'Desenvolvimento de uma nova técnica de reforço com materiais compósitos para estruturas de betão' with the reference of "004/TT/2024". This work was partly financed by FCT / MCTES through national funds (PIDDAC) under the R&D Unit Institute for Sustainability and Innovation in Structural Engineering (ISISE), under reference UIDB/04029/2020, and under the Associate Laboratory Advanced Production and Intelligent Systems ARISE under reference LA/P/0112/2020.

Appendix A

A summary of the database collected from existing compressive tests carried out on FRP-confined concrete circular columns can be found in Table A1.

Appendix B

The experimental FRP-confined concrete N-150C1L specimen tested by Ozbakkaloglu and Vincent [14] was selected as an example to demonstrate the application of the proposed stress-strain model for Type A columns. The specimen has a diameter and height of 152 and 305 mm ($b = 152$ mm, $L = 305$ mm, $\beta_b = 1.01$, and $\beta_L = 2.01$), confined by one CFRP layer ($n_f = 1$). The axial compressive strength of unconfined concrete was 34.6 MPa (f_{c0}

$= 34.6$MPa). The mechanical properties of CFRP were reported as: $t_f = 0.117$mm, $E_f = 251$GPa and $\varepsilon_{fu} = 0.0144$.

- ***Input parameters of the proposed stress-strain relationship***:

$$\varepsilon_{c0} = 0.0011\left(f_{c0}/\beta_L\right)^{0.25} = 0.0011(34.6/2.01)^{0.25} = 0.0022 \quad (4)$$

$$K_L = 2n_f t_f E_f / b = 2 \times 1 \times 0.117 \times 251000/152 = 386.4\text{MPa} \quad (3)$$

$$\rho_K = K_L \varepsilon_{c0}/f_{c0} = 386.4 \times 0.0022/34.6 = 0.025 \quad (2)$$

- ***Calculation of the transition stress and strain***:

$$\frac{f_{ctr}}{f_{c0}} = 0.8{K_L}^{0.05} = 0.8(386.4)^{0.05} = 1.08 \rightarrow f_{ctr} = 37.3\text{MPa} \quad (36)$$

$$\frac{\varepsilon_{ctr}}{\varepsilon_{c0}} = 0.4{f_{c0}}^{0.25}{K_L}^{0.025} = 1.13 \rightarrow \varepsilon_{ctr} = 0.0025 \quad (31)$$

- ***Calculation of the non-dimensional index (RI)***

$$RI = \frac{\rho_K}{6 \times 10^{-5}\alpha_b {f_{c0}}^{1.5}} = \frac{0.025}{6 \times 10^{-5} \times 1.007 \times (34.6)^{1.5}} = 2.04 \quad (1)$$

where $\alpha_b = \sqrt{\beta_b} = 1.007$

- ***Calculation of the stress-strain relation*** $\varepsilon_c \le \varepsilon_{ctr}$***, by*** Eq. (11)

$$f_c = \left[-0.57\left(\frac{\varepsilon_c}{\varepsilon_{ctr}}\right)^{2.5} + 1.57\left(\frac{\varepsilon_c}{\varepsilon_{ctr}}\right)\right] f_{ctr} = \left[-0.57\left(\frac{\varepsilon_c}{0.0025}\right)^{2.5} + 1.57\left(\frac{\varepsilon_c}{0.0025}\right)\right] 37.3$$

Rearranging it gives:

$$f_c = -68 \times 10^6 {\varepsilon_c}^{2.5} + 23.4 \times 10^3 \varepsilon_c$$

- ***Calculation of the stress-strain relation*** $\varepsilon_c \ge \varepsilon_{ctr}$***, by*** Eq. (14)

$$f_c = f_{ctr} + 12.5{K_L}^{0.47}{f_{c0}}^{0.44}(\varepsilon_c - \varepsilon_{ctr}) = 37.3 + 12.5(386.4)^{0.47}(34.6)^{0.44}(\varepsilon_c - 0.0025)$$

Rearranging it gives:

$$f_c = 34.9 + 977.3\varepsilon_c$$

Hence, through the obtained f_c vs ε_c relationships, the axial behavior of the test specimen of N-150C1L can be drawn, as demonstrated in Fig. 12a.

Appendix C

The experimental FRP-confined concrete H2–150C3L specimen tested by Ozbakkaloglu and Vincent [14] was selected as an example to demonstrate the application of the proposed stress-strain model for Type B columns. The specimen has a diameter and height of 152 and 305 mm ($b = 152$ mm, $L = 305$ mm, $\beta_b = 1.01$, and $\beta_L = 2.01$, confined by three CFRP layers ($n_f = 3$). The axial compressive strength of unconfined concrete was 92.5 MPa ($f_{c0} = 92.5$MPa). The mechanical properties of CFRP were reported as: $t_f = 0.117$mm, $E_f = 251$GPa and $\varepsilon_{fu} = 0.0144$.

- ***Input parameters of the proposed stress-strain relationship***:

$$\varepsilon_{c0} = 0.0011\left(f_{c0}/\beta_L\right)^{0.25} = 0.0011(92.5/2.01)^{0.25} = 0.0029 \quad (4')$$

$$K_L = 2n_f t_f E_f / b = 2 \times 3 \times 0.117 \times 251000/152 = 1159.2\text{MPa} \quad (3')$$

$$\rho_K = K_L \varepsilon_{c0}/f_{c0} = 1159.2 \times 0.0029/92.5 = 0.0359 \quad (2')$$

- ***Calculation of the transition stress and strain***:

$$\frac{f_{ctr}}{f_{c0}} = 0.8{K_L}^{0.05} = 0.8(1159.2)^{0.05} = 1.14 \rightarrow f_{ctr} = 105.3\text{MPa} \quad (36')$$

$$\frac{\varepsilon_{ctr}}{\varepsilon_{c0}} = 0.4{f_{c0}}^{0.25}{K_L}^{0.025} = 0.4(92.5)^{0.25}(1159.2)^{0.025} = 1.48 \rightarrow \varepsilon_{ctr} = 0.0042 \quad (31')$$

- ***Calculation of the non-dimensional index (RI)***

$$RI = \frac{\rho_K}{6 \times 10^{-5}\alpha_b {f_{c0}}^{1.5}} = \frac{0.0359}{6 \times 10^{-5} \times 1.007 \times (92.5)^{1.5}} = 0.67 \quad (1')$$

where $\alpha_b = \sqrt{\beta_b} = 1.007$

- ***Calculation of the stress-strain relation $\varepsilon_c \le \varepsilon_{ctr}$, by*** Eq. (11)

$$f_c = \left[-0.57\left(\frac{\varepsilon_c}{\varepsilon_{ctr}}\right)^{2.5} + 1.57\left(\frac{\varepsilon_c}{\varepsilon_{ctr}}\right)\right] f_{ctr} = \left[-0.57\left(\frac{\varepsilon_c}{0.0042}\right)^{2.5} + 1.57\left(\frac{\varepsilon_c}{0.0042}\right)\right] 105.3$$

Rearranging it gives:

$$f_c = -7.14 \times 10^6 {\varepsilon_c}^{2.5} + 57 \times 10^3 \varepsilon_c$$

- ***Calculation of the axial strain of ε_{ci}***

$$\varepsilon_{ci} = (1 - RI)^{-\eta_\varepsilon}\varepsilon_{ci0} = (1 - 0.67)^{-0.84}0.0031 = 0.0079$$

in which

$$\eta_\varepsilon = 0.01 RI^{-0.55}{f_{c0}}^{0.93}{\beta_b}^{-0.4} = 0.01(0.67)^{-0.55}(92.5)^{0.93}(1.01)^{-0.4} = 0.84 \quad (25')$$

- ***Calculation of the reduction factor of λ_1***

$$\lambda_1 = RI^{\eta_1} = (0.67)^{0.71} = 0.75$$

in which

$$\eta_1 = 0.23 RI^{0.6}{f_{c0}}^{0.3}\beta_b = 0.23(0.67)^{0.6}(92.5)^{0.3}1.01 = 0.71 \quad (28')$$

- ***Calculation of the stress-strain relation for $\varepsilon_c \ge \varepsilon_{ctr}$ by*** Eqs. (15), (22) ***and* (26)**

$$f_c = \max\left[f_c^{II}, f_c^{III}\right]$$

in which

$$f_c^{II} = f_{ctr} - 0.425 f_{c0}\frac{\varepsilon_c - \varepsilon_{ctr}}{\varepsilon_{ci} - \varepsilon_{ctr}} = 105.3 - 0.425 \times 92.5 \times \frac{\varepsilon_c - 0.0042}{0.0079 - 0.0042} = 149.9 - 10625\varepsilon_c$$

$$f_c^{III} = \lambda_1 f_{ctr} + 12.5{K_L}^{0.47}{f_{c0}}^{0.44}(\varepsilon_c - \varepsilon_{ctr})$$
$$= 0.75 \times 105 + 12.5(1159)^{0.47}(92.5)^{0.44}(\varepsilon_c - 0.0042) = 68 + 2524\varepsilon_c$$

Hence, through the obtained f_c vs ε_c relationships, the axial behavior of the test specimen of H2–150C3L can be drawn, as demonstrated in Fig. 13a.

Table A1
Summary of the collected database of axial compressive tests

Column Type	Number of Specimens	Statistical Indicators	Geometrical properties		Concrete properties		FRP confinement properties		
			b range (mm)	**L range (mm)**	**f_{c0} range (MPa)**	**ε_{c0} range**	**$n_f \times t_f$ range (mm)**	**E_f range (GPa)**	**ε_{fu} range**
All	**585**	Min.	50	100	20.6	0.0018	0.11	9.5	0.005
		Max.	326	980	204	0.0035	6.40	558	0.094
		Mean	138	279	55.8	0.0024	0.78	171	0.024
		Median	150	300	40.1	0.0023	0.40	236	0.017
		CoV	0.335	0.371	0.731	0.155	1.148	0.577	0.836
Type A	**479**	Min.	50	100	20.6	0.0018	0.11	9.5	0.005
		Max.	300	900	188.2	0.0035	5.10	558	0.094
		Mean	144	291	43.7	0.0023	0.78	174	0.023
		Median	150	300	38.0	0.0023	0.47	236	0.017

(*continued on next page*)

Table A1 (*continued*)

Column Type	Number of Specimens	Statistical Indicators	Geometrical properties		Concrete properties		FRP confinement properties		
			b range (mm)	**L range (mm)**	**f_{c0} range (MPa)**	**ε_{c0} range**	**$n_f \times t_f$ range (mm)**	**E_f range (GPa)**	**ε_{fu} range**
		CoV	0.292	0.325	0.583	0.118	1.088	0.571	0.788
Type B	**106**	Min.	50	100	38.0	0.0023	0.11	9.6	0.009
		Max.	326	980	204.0	0.0035	6.40	244	0.094
		Mean	111	222	112.5	0.0030	0.69	159	0.028
		Median	108	200	112.0	0.0030	0.33	230	0.016
		CoV	0.493	0.547	0.444	0.120	1.465	0.591	0.961

Note: Type A = Stress-strain relation with strain hardening behavior; Type B = Stress-strain relation with partial or integral post-peak strain softening behavior; b = section dimension; L = height of the column; f_{c0} = compressive strength of unconfined concrete; ε_{c0} = axial strain corresponding to f_{c0}, calculated by Eq. (2); n_f = number of FRP layer; t_f = nominal thickness of a FRP layer; E_f = FRP modulus elasticity; ε_{fu} = FRP ultimate tensile strain.

References

[1] N.A. Abdulla, A state-of art-review of materials, methods, and applications of PVC-FRP-confined concrete, Constr. Build. Mater. 363 (2023) 129719.
[2] J.C. Lim, T. Ozbakkaloglu, Hoop strains in FRP-confined concrete columns: experimental observations, Mater. Struct. 48 (2015) 2839–2854.
[3] D.S. De Oliveira, V. Raiz, R. Carrazedo, Experimental study on normal-strength, high-strength and ultrahigh-strength concrete confined by carbon and glass FRP laminates, J. Comp. Constr. 23 (1) (2019) 04018072.
[4] S. Lin, Y.G. Zhao, J. Li, Z.H. Lu, Confining stress path-based compressive strength model of axially loaded FRP-confined columns, J. Comp. Constr. 25 (1) (2021) 04020077.
[5] F. Alrshoudi, H. Abbas, A. Abadel, A. Albidah, A. Altheeb, Y. Al-Salloum, Compression behavior and modeling of FRP-confined high strength geopolymer concrete, Constr. Build. Mater. 283 (2021) 122759.
[6] A.I. Karabinis, T.C. Rousakis, Concrete confined by FRP material: a plasticity approach, Eng. struct. 24 (7) (2002) 923–932.
[7] A. Mirmiran, M. Shahawy, M. Samaan, H.E. Echary, J.C. Mastrapa, O. Pico, Effect of column parameters on FRP-confined concrete, J. Comp. constr. 2 (4) (1998) 175–185.
[8] T.C. Rousakis, A.I. Karabinis, Adequately FRP confined reinforced concrete columns under axial compressive monotonic or cyclic loading, Mater. struct. 45 (2012) 957–975.
[9] M. Nematzadeh, M. Mousavimehr, J. Shayanfar, M. Omidalizadeh, Eccentric compressive behavior of steel fiber-reinforced RC columns strengthened with CFRP wraps: experimental investigation and analytical modeling, Eng. Struct. 226 (2021) 111389.
[10] T.C. Rousakis, Hybrid confinement of concrete by fiber-reinforced polymer sheets and fiber ropes under cyclic axial compressive loading, J. Comp. Constr. *17* (*5*) (2013) *732–743*.
[11] J.A. Barros, D.R. Ferreira, Assessing the efficiency of CFRP discrete confinement systems for concrete cylinders, J. Comp. Constr. *12* (2) (2008) 134–148.
[12] T. Ozbakkaloglu, E. Akin, Behavior of FRP-confined normal-and high-strength concrete under cyclic axial compression, J. Comp. Constr. 16 (4) (2012) 451–463.
[13] H.M. Elsanadedy, Y.A. Al-Salloum, S.H. Alsayed, R.A. Iqbal, Experimental and numerical investigation of size effects in FRP-wrapped concrete columns, Constr. Build. Mater. 29 (2012) 56–72.
[14] T. Ozbakkaloglu, T. Vincent, Axial compressive behavior of circular high-strength concrete-filled FRP tubes, J. comp. constr. 18 (2) (2014) 04013037.
[15] D.Y. Wang, Z.Y. Wang, S.T. Smith, T. Yu, Size effect on axial stress-strain behavior of CFRP-confined square concrete columns, Constr. Build. Mater. 118 (2016) 116–126.
[16] J. Shayanfar, J.A. Barros, Design-oriented model of unified character to determine softening/hardening stress-strain behavior of FRP-confined concrete columns of general cross-section, J. comp. constr. (2024), https://doi.org/10.1061/JCCOF2/CCENG-4772..
[17] J.J. Zeng, Y.Y. Ye, W.Y. Gao, S.T. Smith, Y.C. Guo, Stress-strain behavior of polyethylene terephthalate fiber-reinforced polymer-confined normal-, high-and ultra high-strength concrete, J. Build. Eng. 30 (2020) 101243.
[18] J.J. Zeng, J.D. Chen, J. Liao, W.J. Chen, Y. Zhuge, Y. Liu, Behavior of ultra-high performance concrete under true tri-axial compression, Constr. Build. Mater. 411 (2024) 134450.
[19] R. Eid, N. Roy, P. Paultre, Normal-and high-strength concrete circular elements wrapped with FRP composites, J. comp. constr. 13 (2) (2009) 113–124.
[20] Y. Wei, Y.F. Wu, Experimental study of concrete columns with localized failure, J. Comp. Constr. 20 (5) (2016) 04016032.
[21] J. Shayanfar, J.A. Barros, M. Rezazadeh, Generalized Analysis-oriented model of FRP confined concrete circular columns, Comp. Struct. 270 (2021) 114026.
[22] A. Fallahpour, G.D. Nguyen, T. Vincent, T. Ozbakkaloglu, Investigation of the compressive behavior and failure modes of unconfined and FRP-confined concrete using digital image correlation, Comp. Struct. 252 (2020) 112642.
[23] J. Shayanfar, M. Rezazadeh, J.A. Barros, Analytical model to predict dilation behavior of FRP confined circular concrete columns subjected to axial compressive loading, J. Comp. Constr. 24 (6) (2020) 04020071.
[24] J. Wang, H. Xiao, L. Lu, J. Yang, S. Lu, J. Shayanfar, Axial stress-strain model for concrete in partially FRP wrapped reinforced concrete columns, Constr. Build. Mater. 416 (2024) 135028.
[25] T. Vincent, T. Ozbakkaloglu, Influence of concrete strength and confinement method on axial compressive behavior of FRP confined high-and ultra high-strength concrete, Comp. Part B: Eng. 50 (2013) 413–428.
[26] U. Demir, M. Ispir, Y. Sahinkaya, G. Arslan, A. Ilki, Axial behavior of noncircular high-performance fiber-reinforced cementitious composite members externally jacketed by CFRP sheets, J. Comp. Constr. 23 (4) (2019) 04019022.
[27] J. Liao, K.Y. Yang, J.J. Zeng, W.M. Quach, Y.Y. Ye, L. Zhang, Compressive behavior of FRP-confined ultra-high performance concrete (UHPC) in circular columns, Eng. Struct. 249 (2021) 113246.
[28] J. Zhou, F. Bi, Z. Wang, J. Zhang, Experimental investigation of size effect on mechanical properties of carbon fiber reinforced polymer (CFRP) confined concrete circular specimens, Constr. Build. Mater. 127 (2016) 643–652.
[29] S. Pessiki, K.A. Harries, J.T. Kestner, R. Sause, J.M. Ricles, Axial behavior of reinforced concrete columns confined with FRP jackets, J. comp. Constr. 5 (4) (2001) 237–245.
[30] L. Fan, L. Jin, X. Du, Modeling of size effect on compressive behavior of CFRP-confined rectangular RC columns: Influence of corner radius and aspect ratio, Comp. Struct. 304 (2023) 116400.
[31] R. Jamatia, A. Deb, Size effect in FRP-confined concrete under axial compression, J. Comp. Constr. 21 (6) (2017) 04017045.
[32] T.C. Rousakis, T.D. Rakitzis, A.I. Karabinis, Design-oriented strength model for FRP-confined concrete members, J. Comp. Constr. *16* (*6*) (2012) *615–625*.
[33] D.A. Moran, C.P. Pantelides, Stress-strain model for fiber-reinforced polymer-confined concrete, J. comp. constr. *6* (*4*) (2002) *233–240*.
[34] L. Lam, J.G. Teng, Design-oriented stress–strain model for FRP-confined concrete. Constr. build. mater. 17 (6-7) (2003) 471–489.
[35] T. Jiang, J.G. Teng, Analysis-oriented stress–strain models for FRP–confined concrete. Eng. Struct. 29 (11) (2007) 2968–2986.
[36] J.G. Teng, T. Jiang, L. Lam, Y.Z. Luo, Refinement of a design-oriented stress–strain model for FRP-confined concrete, J. comp. constr. 13 (4) (2009) 269–278.
[37] Y.Y. Wei, Y.F. Wu, Unified stress–strain model of concrete for FRP-confined columns. Constr. Build. Mater. 26 (1) (2012) 381–392.
[38] Y.G. Cao, C. Jiang, Y.F. Wu, Cross-sectional unification on the stress-strain model of concrete subjected to high passive confinement by fiber-reinforced polymer, Polymers 8 (5) (2016) 186.
[39] A. Fallahpour, T. Ozbakkaloglu, T. Vincent, Simplified design-oriented axial stress-strain model for FRP-confined normal-and high-strength concrete, Eng. Struct. 175 (2018) 501–516.
[40] J. Shayanfar, J.A. Barros, M. Rezazadeh, Analytical model to predict axial stress-strain behavior of heat-damaged unreinforced concrete columns wrapped by FRP jacket, Eng. Struct. 289 (2023) 116244.
[41] J. Shayanfar, J.A. Barros, M. Rezazadeh, Cross-sectional and confining system unification on peak compressive strength of FRP confined concrete. Struct. Concrete 24 (1) (2023) 1531–1545.
[42] J. Shayanfar, H.J. Kafshgarkolaei, J.A. Barros, M. Rezazadeh, Unified strength model for FRP confined heat-damaged circular and square concrete columns, Comp. Struct. 307 (2023) 116647.
[43] J. Shayanfar, J.A. Barros, M. Rezazadeh, Stress–strain model for FRP confined heat-damaged concrete columns. Fire Safety J. 136 (2023) 103748.
[44] J. Liao, J.J. Zeng, Q.M. Gong, W.M. Quach, W.Y. Gao, L. Zhang, Design-oriented stress-strain model for FRP-confined ultra-high performance concrete (UHPC), Constr. build. mater. 318 (2022) 126200.
[45] J. Shayanfar, J.A. Barros, M. Rezazadeh, Unified model for fully and partially FRP confined circular and square concrete columns subjected to axial compression, Eng. Struct. 251 (2022) 113355.
[46] J. Shayanfar, J.A. Barros, M. Abedi, M. Rezazadeh, Unified compressive strength and strain ductility models for fully and partially FRP-confined circular, square, and rectangular concrete columns, J. Comp. Constr. 27 (6) (2023) 04023053.
[47] J. Wang, S. Lin, Y.G. Zhao, Stress path-based compressive strength model of FRP-confined recycled aggregate concrete, Constr. Build. Mater. 440 (2024) 137437.
[48] T. Ozbakkaloglu, J.C. Lim, T. Vincent, FRP-confined concrete in circular sections: Review and assessment of stress–strain models, Eng. Struct. 49 (2013) 1068–1088.

[49] L. Huang, C. Gao, L. Yan, B. Kasal, G. Ma, H. Tan, Confinement models of GFRP-confined concrete: statistical analysis and unified stress–strain models, J. Reinforced Plast. Comp. 35 (11) (2016) 867–891.
[50] J. Liao, J.J. Zeng, Y. Zhuge, Y. Zheng, G. Ma, L. Zhang, FRP-Confined Concrete Columns with a Stress Reduction-Recovery Behavior: a state-of-the-art review, design recommendations and model assessments, Compos. Struct. (2023) 117313.
[51] J.J. Wang, S.S. Zhang, X.F. Nie, T. Yu, Compressive behavior of FRP-confined ultra-high performance concrete (UHPC) and ultra-high performance fiber reinforced concrete (UHPFRC), Compos. Struct. 312 (2023) 116879.
[52] W. Li, W. Li, Y. Lu, B. Hu, Y. Zhou, H. Wu, P. Wang, L. Ke, J. Yu, Axial compressive behavior and failure mechanism of CFRP partially confined ultra-high performance concrete (UHPC), Constr. Build. Mater. 426 (2024) 136104.
[53] J. Shayanfar, J.A. Barros, M. Rezazadeh, Stress–strain model for FRP-confined circular concrete columns developing structural softening behavior, J. Compos. Constr. 28 (1) (2024) 04023065.
[54] J. Shayanfar, J.A. Barros, M. Rezazadeh, Analysis-oriented model for partially FRP-and-steel-confined circular RC columns under compression, Eng. Struct. 276 (2023) 115330.
[55] J.G. Dai, Y.L. Bai, J.G. Teng, Behavior and modeling of concrete confined with FRP composites of large deformability, J. Compos. Constr. *15* (*6*) (2011) *963–973*.
[56] M. Samaan, A. Mirmiran, M. Shahawy, Model of concrete confined by fiber composites, J. Struct. Eng. 124 (9) (1998) 1025–1031.
[57] G. Lin, T. Yu, J.G. Teng, Design-oriented stress–strain model for concrete under combined FRP-steel confinement, J. Compos. Constr. 20 (4) (2016) 04015084.
[58] ACI 440.2R-17. Guide for the design and construction of externally bonded FRP systems for strengthening concrete structures; American Concrete Institute (ACI): Farmington Hills MI USA 2017.
[59] Fib Bulletin 90. Externally applied FRP reinforcement for concrete structures. Task Group 5. 1, International Federation for Structural Concrete 2019.
[60] Z. Wang, D. Wang, S.T. Smith, D. Lu, Experimental testing and analytical modeling of CFRP-confined large circular RC columns subjected to cyclic axial compression, Eng. Struct. 40 (2012) 64–74.
[61] T.D. Fanaradelli, T.C. Rousakis, 3D finite element pseudodynamic analysis of deficient RC rectangular columns confined with fiber reinforced polymers under axial compression, Polymers 12 (11) (2020) 2546.
[62] T. Ozbakkaloglu, Axial compressive behavior of square and rectangular high-strength concrete-filled FRP tubes, J. Compos. Constr. 17 (1) (2013) 151–161.
[63] Y. Wang, P. Liu, Q. Cao, G. Chen, B. Wan, Z. Wei, Y.L. Bai, Comparison of monotonic axial compressive behavior of rectangular concrete confined by FRP with different rupture strains, Constr. Build. Mater. 299 (2021) 124241.
[64] T.C. Triantafillou, E. Choutopoulou, E. Fotaki, M. Skorda, M. Stathopoulou, K. Karlos, FRP confinement of wall-like reinforced concrete columns, Mater. Struct. 49 (2016) 651–664.
[65] J. Shayanfar, J.A. Barros, M. Rezazadeh, Design-oriented stress-strain model for RC columns with dual FRP-steel confinement mechanism, Compos. Struct. (2023) 117821.